

# COMPRESSIVE ACQUISITION OF DYNAMICAL SCENES

ASWIN C. SANKARANARAYANAN\*, PAVAN K. TURAGA†, RAMA CHELLAPPA‡, AND  
RICHARD G. BARANIUK\*

**Abstract.** Compressive sensing (CS) is a new approach for the acquisition and recovery of sparse signals and images that enables sampling rates significantly below the classical Nyquist rate. Despite significant progress in the theory and methods of CS, little headway has been made in compressive video acquisition and recovery. Video CS is complicated by the ephemeral nature of dynamic events, which makes direct extensions of standard CS imaging architectures and signal models difficult. In this paper, we develop a new framework for video CS for dynamic textured scenes that models the evolution of the scene as a linear dynamical system (LDS). This reduces the video recovery problem to first estimating the model parameters of the LDS from compressive measurements, and then reconstructing the image frames. We exploit the low-dimensional dynamic parameters (the state sequence) and high-dimensional static parameters (the observation matrix) of the LDS to devise a novel compressive measurement strategy that measures only the dynamic part of the scene at each instant and accumulates measurements over time to estimate the static parameters. This enables us to lower the compressive measurement rate considerably. We validate our approach with a range of experiments involving both video recovery, sensing hyper-spectral data, and classification of dynamic scenes from compressive data. Together, these applications demonstrate the effectiveness of the approach.

**Key words.** Compressive sensing, Linear dynamical system, Video compressive sensing, Hyper-spectral imaging

**1. Introduction.** The Shannon-Nyquist theorem dictates that to sense features at a particular frequency, we need to sample uniformly at twice that rate. For some applications, this sampling rate might be too high and/or redundant; in modern digital cameras, invariably, the sensed image is compressed immediately without much loss in quality. For some applications, such as high speed imaging and sensing in the non-visual spectrum, camera/sensor designs based on the Shannon-Nyquist theorem lead to impractical and costly designs. Part of the reason for this is that the Shannon-Nyquist sampling theory does not exploit any structure in the sensed signal beyond that of band-limitedness. Signals with redundant structures can potentially be sensed more parsimoniously. This is the key idea underlying a new field called *compressive sensing* (CS) [7]. When the signal of interest exhibits a sparse representation, CS enables sensing at measurement rates below the Nyquist rate. Indeed, signal recovery is possible from a number of measurements that is proportional to the sparsity level of the signal, as opposed to its bandwidth.

In this paper, we consider the problem of sensing *videos* compressively. We are interested in this problem motivated by the success of video compression algorithms, which indicates that videos are highly redundant. Bridging the gap between compression and sensing can lead to compelling camera designs that significantly reduce the amount of data sensed and enable designs for application domains where sensing is inherently costly.

Video CS is challenging for two main reasons:

---

\*A. C. Sankaranarayanan and R. G. Baraniuk are with the Department of Electrical and Computer Engineering at the Rice University, Houston, TX. Email: {saswin, richb}@rice.edu. Web: dsp.rice.edu

†P. K. Turaga is with the Arts Media and Engineering Department, Arizona State University, Tempe, AZ. Email: pturaga@asu.edu

‡R. Chellappa is with the Department of Electrical and Computer Engineering at the University of Maryland, College Park, MD. Email: rama@cfar.umd.edu.

- **Ephemeral nature of videos:** The scene changes during the measurement process; moreover, we cannot obtain additional measurements of an event after it has occurred.
- **High-dimensional signals:** Videos are significantly higher-dimensional than images. This makes the recovery process computationally intensive.

One way to address these challenges is to restrict the scope to estimation of parametric models that are suitable for a broad class of videos.

In this paper, we develop a CS framework for videos modeled as linear dynamical systems (LDSs) — motivated, in part, by the extensive use of such models in characterizing dynamic textures [11, 15, 32], activity modeling, and video clustering [35]. Parametric models, like LDSs, offer lower dimensional representations for otherwise high-dimensional videos. This restricts the number of free parameters that need to be estimated and, as a consequence, reduces the amount of data that needs to be sensed. In the context of video sensing, LDSs offer interesting tradeoffs by characterizing the video signal using a mix of dynamic/time-varying parameters and static/time-invariant parameters. Further, the generative nature of LDSs provides a prior for the evolution of the video in both forward and reverse time. To a large extent, this property helps us circumvent the challenges presented by the ephemeral nature of videos.

The paper makes the following contributions. We propose a framework called *CS-LDS* for video acquisition using an LDS model coupled with sparse priors for the parameters of the LDS model. The core of the framework is a *two-step measurement strategy* that enables the recovery of the LDS parameters from compressive measurements by solving a sequence of linear and convex problems. We demonstrate that CS-LDS is capable of sensing videos and hyper-spectral data with far fewer measurements than the Nyquist rate. Finally, the LDS parameters form an important class of features for activity recognition and scene analysis, thereby making our camera designs purposive [24] as well.

## 2. Background.

**2.1. Compressive sensing.** CS deals with the recovery of a signal  $\mathbf{y} \in \mathbb{R}^N$  from undersampled linear measurements of the form  $\mathbf{z} = \Phi\mathbf{y} + \mathbf{e}$ , where  $\Phi \in \mathbb{R}^{M \times N}$  is the measurement matrix,  $M < N$ , and  $\mathbf{e}$  is the measurement noise [7, 14]. Estimating  $\mathbf{y}$  from the measurements  $\mathbf{z}$  is ill-conditioned, since the linear system formed by  $\mathbf{z} = \Phi\mathbf{y}$  is under-determined. CS works under the assumption that the signal  $\mathbf{y}$  is sparse in a basis  $\Psi$ ; that is, the signal  $\mathbf{s}$ , defined as  $\mathbf{y} = \Psi\mathbf{s}$ , has at most  $K$  non-zero components. Exploiting the sparsity of  $\mathbf{s}$ , the signal  $\mathbf{y}$  can be recovered exactly from  $M = O(K \log(N/K))$  measurements provided the matrix  $\Phi\Psi$  satisfies the so-called *restricted isometry property* (RIP) [4]. In particular, when  $\Psi$  is an orthonormal basis and the entries of the matrix  $\Phi$  are i.i.d. samples from a sub-Gaussian distribution, the product  $\Phi\Psi$  satisfies the RIP. Further, the signal  $\mathbf{y}$  can be recovered from  $\mathbf{z}$  by solving a convex problem of the form

$$\min \|\mathbf{s}\|_1 \text{ subject to } \|\mathbf{z} - \Phi\Psi\mathbf{s}\|_2 \leq \epsilon \quad (1)$$

where  $\epsilon$  is an upper bound on the measurement noise  $\mathbf{e}$ . It can be shown that the solution to (1) is with high probability the  $K$ -sparse solution that we seek. The theoretical guarantees of CS have been extended to *compressible* signals, where the sorted coefficients of  $\mathbf{s}$  decay rapidly according to a power-law [21].

There exist a wide range of algorithms to solve (1) under various approximations or reformulations [7, 36]. Greedy techniques such as Orthogonal Matching Pursuit [27]

and CoSAMP [25] solve the sparse approximation problem efficiently with strong convergence properties and low computational complexity. It is also simple to impose structural constraints such as block sparsity into CoSAMP giving variants such as model-based CoSAMP [3].

**2.2. Video compressive sensing.** In video CS, the goal is to sense a time-varying scene using compressive measurements of the form  $\mathbf{z}_t = \Phi_t \mathbf{y}_t$ , where  $\mathbf{z}_t$ ,  $\Phi_t$  and  $\mathbf{y}_t$  are the compressive measurements, the measurement matrix and the video frame at time  $t$ , respectively. Given the sequence of compressive measurements  $\mathbf{z}_{1:T} = \{\mathbf{z}_1, \mathbf{z}_2, \dots, \mathbf{z}_T\}$ , our goal is to recover the video frames  $\mathbf{y}_{1:T} = \{\mathbf{y}_1, \mathbf{y}_2, \dots, \mathbf{y}_T\}$ . There are currently two fundamentally different imaging architectures for video CS: the single pixel camera (SPC) and the programmable pixel camera. The SPC [16] uses a single or a small number of sensing elements. Typically, a photo-detector is used to obtain a single measurement at each time instant of the form  $\mathbf{z}_t = \phi_t^T \mathbf{y}_t$ , where  $\phi_t$  is a pseudo-random vector of 0s and 1s. Typically, under an assumption of a slowly varying scene, consecutive measurements from the SPC are grouped as measurements of the same video frame. This assumption works only when the scene motion is small or when the number of measurements associated with a frame is small. The SPC provides complete freedom in the spatial multiplexing of pixels; however, there is no temporal multiplexing. In contrast, programmable pixel cameras [22, 30, 41] use a full frame sensor array; during each exposure of the sensor array, the shutter at each pixel is temporally modulated. This enables extensive temporal multiplexing but a limited amount of spatial multiplexing. A key advantage of SPC-based designs is that they can operate efficiently at wavelengths (such as the far infrared) that require exotic detectors; in such cases, building a full frame sensor can be prohibitively expensive.

To date, recovery algorithms for the SPC have used various signal models to reconstruct the sensed scene. Wakin et al. [42] use 3D wavelets as the sparsifying basis for recovering videos from compressive measurements. Park and Wakin [26] use a coarse-to-fine estimation framework wherein the video, reconstructed at a coarse scale, is used to estimate motion vectors that are subsequently used to design dictionaries for reconstruction at a finer scale. Vaswani [38] and Vaswani and Lu [39] use a sequential framework that exploits the similarity of support of the signal between adjacent frames of a video. Under this model, a frame of video is reconstructed using a linear inversion over the support at the previous time instant and a small-scale CS recovery over the residue to detect components beyond the known support. Cevher et al. [9] provide a CS framework for directly sensing innovations over a static scene thereby enabling background subtraction from compressive measurements.

**2.3. Linear dynamical system model for video sequences.** Linear dynamical systems (LDSs) represent an important class of parametric models for time-series data. A wide variety of spatio-temporal signals have often been modeled as realizations of LDSs. These include dynamic textures [15], traffic scenes [11], and human activities [35].

Under an LDS model, the evolution of the video frames  $\mathbf{y}_t$  is described in terms of a hidden state space

$$\begin{aligned}\mathbf{y}_t &= C\mathbf{x}_t + \mathbf{w}_t, \\ \mathbf{x}_{t+1} &= A\mathbf{x}_t + \mathbf{v}_t\end{aligned}$$

where  $\mathbf{x}_t \in \mathbb{R}^d$  is the state vector at time  $t$ ,  $d$  is the dimension of the state space,  $A \in \mathbb{R}^{d \times d}$  is the state transition matrix,  $C \in \mathbb{R}^{N \times d}$  is the observation matrix,  $Q$  and

$R$  are the process and observation noise covariance matrices, respectively. For the videos of interest in this paper,  $d \ll N$ .

LDSs are parameterized by the matrix pair  $(C, A)$ . Note that the choice of  $C$  and the state sequence  $\mathbf{x}_{1:T}$  is unique only up to a  $d \times d$  linear transformation given the inherent ambiguities in the notion of a state space. In particular, given *any* invertible  $d \times d$  matrix  $L$ , the LDS defined by  $(C, A)$  with the state sequence  $\mathbf{x}_{1:T}$  is equivalent to the LDS defined by  $(CL, L^{-1}AL)$  with the state sequence  $L^{-1}\mathbf{x}_{1:T} = \{L^{-1}\mathbf{x}_1, L^{-1}\mathbf{x}_2, \dots, L^{-1}\mathbf{x}_T\}$ . This lack of uniqueness has implications that we will touch upon later in Section 5.

Given a video sequence, the most common approach to fitting an LDS model is to first estimate a lower-dimensional embedding of the observations via principal component analysis (PCA) and then learn the temporal dynamics captured in  $\mathbf{x}_t$ , and equivalently  $A$ . The most popular model estimation algorithms are N4SID [37], PCA-ID [34], and expectation-maximization (EM) [11]. N4SID is a subspace identification algorithm that provides an asymptotically optimal solution for the model parameters. However, for large problems the computational requirements make this method prohibitive. PCA-ID [34] is a sub-optimal solution to the learning problem. It makes the assumption that filtering in space and time are separable, which makes it possible to estimate the parameters of the model very efficiently via PCA. The learning problem can also be posed as a maximum likelihood estimation of the model parameters that maximize the likelihood of the observations, which can be solved by EM [11].

**3. CS-LDS Architecture.** We provide a high level overview of our proposed framework for video CS; the goal here is to build a CS framework, implementable on the SPC, for videos that are modeled as LDSs. We flesh out the details in Sections 4 and 5. This amounts to estimating the LDS parameters from compressive measurements, i.e, we seek to recover the model parameters  $C$  and  $\mathbf{x}_{1:T}$  given compressive measurements of the form  $\mathbf{z}_t = \Phi_t \mathbf{y}_t = \Phi_t C \mathbf{x}_t$ . We recall that  $C$  is the time-invariant observation matrix of the LDS, and  $\mathbf{y}_t$  and  $\mathbf{x}_t$  are the video frame and the state at time  $t$ , respectively. The compressive measurements  $\mathbf{z}_{1:T}$  are hence expressed as bilinear terms in the unknown parameters  $C$  and  $\mathbf{x}_{1:t}$ . Handling bilinear unknowns typically requires non-convex optimization techniques thereby invalidating conventional CS recovery algorithms. To avoid this, we propose a two-step sensing method that is specifically designed to address the bilinearity; we refer to this sensing method and its associated recovery algorithm as the *CS-LDS* framework [33].

**Measurement model:** We summarize the CS-LDS measurement model as follows. At time  $t$ , we take two sets of measurements:

$$\mathbf{z}_t = \begin{pmatrix} \check{\mathbf{z}}_t \\ \tilde{\mathbf{z}}_t \end{pmatrix} = \begin{bmatrix} \check{\Phi} \\ \tilde{\Phi}_t \end{bmatrix} \mathbf{y}_t = \Phi_t \mathbf{y}_t, \quad (2)$$

where  $\check{\mathbf{z}}_t \in \mathbb{R}^{\check{M}}$  and  $\tilde{\mathbf{z}}_t \in \mathbb{R}^{\tilde{M}}$  such that the total number of measurements at each frame is  $M = \check{M} + \tilde{M}$ .<sup>1</sup> The measurement matrix in (2) is composed of two distinct components: a *time-invariant* part  $\check{\Phi}$  and a *time-varying* part  $\tilde{\Phi}_t$ . We denote by  $\check{\mathbf{z}}_t$  the *common* measurements and by  $\tilde{\mathbf{z}}_t$  the *innovation* measurements.

<sup>1</sup>The SPC obtains only one measurement at each time instant. Multiple measurements for a video frame are obtained by grouping consecutive measurements from the SPC. When  $M$  is small, compared to the sampling rate of the SPC, this is an acceptable approximation especially for slowly varying scenes.

We solve for the LDS parameters in two steps. First, we obtain an estimate of the state sequence using only the common measurements  $\tilde{\mathbf{z}}_{1:T}$ . Second, we use this state sequence estimate to recover the observation matrix  $C$  using the innovation measurements.

**State sequence estimation:** We recover the state sequence  $\mathbf{x}_{1:T}$  using only the common measurements  $\tilde{\mathbf{z}}_{1:T}$ . The key idea is that when  $\mathbf{y}_{1:T}$  form the observations of an LDS with system matrices  $(C, A)$ , the measurements  $\tilde{\mathbf{z}}_{1:T}$  form the observations of an LDS with system matrices  $(\tilde{\Phi}C, A)$ . Estimation of the state sequence now can be mapped to a simple exercise in system identification. In particular, an estimate of the state sequence can be obtained by the singular value decomposition (SVD) of the block-Hankel matrix

$$\text{Hank}(\tilde{\mathbf{z}}_{1:T}, d) = \begin{bmatrix} \tilde{\mathbf{z}}_1 & \tilde{\mathbf{z}}_2 & \cdots & \cdots & \tilde{\mathbf{z}}_{T-d+1} \\ \tilde{\mathbf{z}}_2 & \ddots & \ddots & & \tilde{\mathbf{z}}_{T-d+2} \\ \vdots & \ddots & \ddots & \ddots & \vdots \\ \vdots & & \ddots & \ddots & \vdots \\ \tilde{\mathbf{z}}_d & \cdots & \cdots & \tilde{\mathbf{z}}_{T-1} & \tilde{\mathbf{z}}_T \end{bmatrix}. \quad (3)$$

Given the  $\text{SVD}(\text{Hank}(\tilde{\mathbf{z}}_{1:T}, d)) = U_H S_H V_H^T$ , the state sequence estimate is given by

$$[\hat{\mathbf{x}}_{1:T}] = S_H V_H^T.$$

In Section 4, we leverage results from system identification to analyze the properties of this particular estimate as well as characterize the number of measurements  $\tilde{M}$  required.

**Observation matrix estimation:** Given knowledge of the state sequence, the relationship between the observation matrix  $C$  and the innovation measurements is linear, i.e.,  $\tilde{\mathbf{z}}_t = \tilde{\Phi}_t C \mathbf{x}_t$ . In addition,  $C$  is *time-invariant*. Hence, we can accumulate innovation measurements over a duration of time to stably reconstruct  $C$ . This significantly reduces the number of innovation measurements  $\tilde{M}$  required at *each* frame. This is especially important in the context of sensing videos, since the scene changes as we acquire measurements. Hence, requiring fewer measurements for each reconstructed frame of the video implies less error due to motion blur.

Using the estimates of the state sequence  $\hat{\mathbf{x}}_{1:T}$ , we can recover  $C$  by solving the following convex problem:

$$\min \sum_{i=1}^d \|\Psi^T \mathbf{c}_i\|_1 \quad \text{s.t.} \quad \forall t, \|\tilde{\mathbf{z}}_t - \tilde{\Phi}_t C \hat{\mathbf{x}}_t\|_2 \leq \epsilon, \quad (4)$$

where  $\mathbf{c}_i$  denotes the  $i$ -th column of  $C$  and  $\Psi$  is a sparsifying basis for the columns of  $C$ . However, as we show later in Section 5.2, ambiguities in the estimation of the state sequence induce a structured sparsity pattern in the support of  $C$ . The convex program (4) can be modified to incorporate such constraints. In addition to this, in Section 5, we also propose a greedy alternative for solving a variant of the convex program.

To summarize (see Figure 1), the two-step measurement process described in (2) enables a two-step recovery. First, we obtain an estimate of the state sequence using SVD on just the common measurements. Second, we use the state sequence estimate for recovering the observation matrix using a convex program. The details of these two steps are discussed in the next two sections.

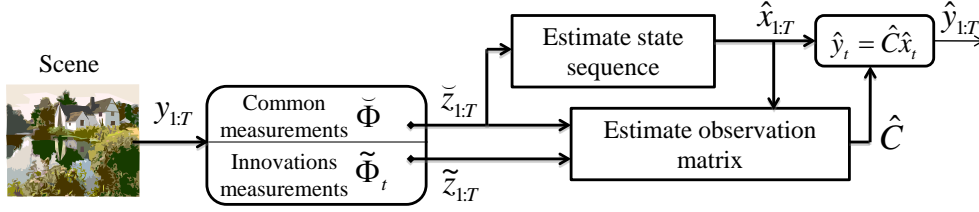


FIG. 1. Block diagram of the CS-LDS framework.

**4. Estimating the state sequence.** In this section, we discuss methods to estimate the state sequence  $\mathbf{x}_{1:T}$  from the compressive measurements  $\check{\mathbf{z}}_{1:T}$ . In particular, we seek to establish sufficient conditions under which the state sequence can be estimated reliably.

**4.1. Observability of the state sequence.** Consider the compressive measurements given by

$$\check{\mathbf{z}}_t = \check{\Phi} y_t + \omega_t, \quad (5)$$

where  $\check{\mathbf{z}}_t \in \mathbb{R}^{\check{M}}$  are the compressive measurements at time  $t$ ,  $\check{\Phi} \in \mathbb{R}^{\check{M} \times N}$  is the corresponding measurement matrix, and  $\omega_t \in \mathbb{R}^{\check{M}}$  is the measurement noise. Note that  $\check{\Phi}$  is time-invariant; hence, (5) is a part of the measurement model described in (2) relating to the common measurements. A key observation is that, when  $\mathbf{y}_{1:T}$  form the observations of an LDS defined by  $(C, A)$ , the compressive measurement sequence  $\check{\mathbf{z}}_{1:T}$  forms an LDS as well; that is,

$$\begin{aligned} \check{\mathbf{z}}_t &= \check{\Phi} y_t + \omega = \check{\Phi} C \mathbf{x}_t + \omega'_t, \\ \mathbf{x}_t &= A \mathbf{x}_{t-1} + w_t. \end{aligned}$$

The LDS associated with  $\check{\mathbf{z}}_{1:T}$  is parameterized by the system matrices  $(\check{\Phi}C, A)$ . Estimating the state sequence from the observations of an LDS is possible only when the LDS is *observable* [5]. Thus, it is important to consider the question of observability of the LDS parameterized by  $(\check{\Phi}C, A)$ .<sup>2</sup>

**DEFINITION 4.1** (Observability of an LDS [5]). *An LDS is observable if, for any possible state sequence, the current state can be estimated from a finite number of observations.*

**LEMMA 4.2** (Test for observability of an LDS [5]). *An LDS defined by the system matrices  $(C, A)$  and of state space dimension  $d$  is observable if and only if the observability matrix*

$$(O(C, A))^T = [C^T (CA)^T (CA^2)^T \cdots (CA^{d-1})^T]^T \quad (6)$$

*is full rank.*

A necessary condition for the observability of the LDS defined by  $(\check{\Phi}C, A)$  is that the LDS defined by  $(C, A)$  is observable. However, for the LDSs we consider in this

<sup>2</sup>Observability of LDSs in the context of CS has been studied earlier by Wakin et al. [43], who consider the scenario when the observation matrix  $C$  is randomly generated and the state vector  $\mathbf{x}_0$  at  $t = 0$  is sparse. In contrast, the analysis we present is for a non-sparse state vector.

paper,  $N \gg d$ ; for such systems, the LDS defined by  $(C, A)$  is observable. Given this assumption, we consider the observability of the LDS parameterized by  $(\check{\Phi}C, A)$  next.

**LEMMA 4.3.** *For  $N > d$ , the LDS defined by  $(\check{\Phi}C, A)$  is observable, with high probability, if  $\check{M} \geq d$  and the entries of the matrix  $\check{\Phi}$  are sampled i.i.d. from a sub-Gaussian distribution.*

*Proof.* This is established by proving that  $\text{rank}(\check{\Phi}C) = d$  when  $\check{M} \geq d$ . Assume that  $\text{rank}(\check{\Phi}C) < d$ , i.e.,  $\exists \alpha \in \mathbb{R}^d$  such that  $\check{\Phi}C\alpha = 0, \alpha \neq 0$ . Let  $\phi^T$  be a row of  $\check{\Phi}$ . The event that  $\phi^T C\alpha = 0$  is one of negligible probability when the elements of  $\phi$  are assumed to be i.i.d. according to a sub-Gaussian distribution such as Gaussian or Bernoulli. Hence, with high probability  $\text{rank}(\check{\Phi}C) = d$  when  $\check{M} \geq d$ .  $\square$

Observability is the key criterion for recovering the state sequence from the common measurements. When the LDS associated with the common measurements is observable, we can estimate the state sequence — up to a linear transformation — by factorizing the block Hankel matrix  $\text{Hank}(\check{\mathbf{z}}_{1:T}, d)$  in (3).  $\text{Hank}(\check{\mathbf{z}}_{1:T}, d)$  can be written as

$$\text{Hank}(\check{\mathbf{z}}_{1:T}, d) = O(\check{\Phi}C, A)[\mathbf{x}_1 \ \mathbf{x}_2 \ \cdots \ \mathbf{x}_{T-d+1}].$$

Hence, when the observability matrix  $O(\check{\Phi}C, A)$  is full rank, we can recover the state sequence by factoring the Hankel matrix using the SVD. Suppose the SVD of the Hankel matrix is  $\text{Hank}(\check{\mathbf{z}}_{1:T}, d) = USV^T$ . Then, the estimate of the state sequence is obtained by

$$[\hat{\mathbf{x}}_{1:T-d+1}] = S_d V_d^T, \quad (7)$$

where  $S_d$  is the diagonal matrix containing the  $d$ -largest singular values in  $S$ , and  $V_d$  is the matrix composed of the right singular vectors corresponding to these singular values. The estimate of the state sequence obtained from SVD differs from its true value by a linear transformation. This is a fundamental ambiguity that stems from the lack of uniqueness in the definition of the state space (see Section 2.3). The state sequence estimate in (7) can be improved, especially for high levels of measurement noise, by using system identification techniques mentioned in Section 2.3. However, the simplicity of this estimate makes it amenable for further analysis.

When  $\check{M} > d$ , we can choose to factorize a smaller-sized Hankel matrix  $\text{Hank}(\check{\mathbf{z}}_{1:T}, q)$  provided  $q > d/\check{M}$ . Note that when  $q = 1$ , we do not enforce the constraints provided by the state transition model, thereby simply reducing the LDS to a linear system. For  $q > 1$ , we enforce the state transition model over  $q$  successive time instants; i.e., we enforce

$$\mathbf{x}_t = A\mathbf{x}_{t-1} = A^2\mathbf{x}_{t-2} = \cdots = A^{q-1}\mathbf{x}_{t-q+1}, \quad q \leq t \leq T.$$

Larger values of  $q$  lead to smoother state sequences, since the estimates conform to the state transition model for longer durations.

We next study the observability properties of specific classes of interesting LDSs and the conditions on  $\check{\Phi}$  under which the observability of  $(\check{\Phi}C, A)$  holds.

**4.2. Case:  $\check{M} = 1$ .** A particularly interesting scenario is when we obtain exactly one common measurement for each video frame. For such a scenario,  $\check{M} = 1$  and, hence, the measurement matrix can be written as a row-vector:  $\check{\Phi} = \phi^T \in \mathbb{R}^{1 \times N}$ . We now establish conditions when the observability matrix  $O(\phi^T C, A)$  is full rank for this

particular scenario. Let  $\check{\mathbf{c}} = (\phi^T C)^T = C^T \phi$  and  $B = A^T$ . We seek a condition when the observability matrix or equivalently its transpose

$$(O(\check{\mathbf{c}}^T, B^T))^T = [\check{\mathbf{c}} \ B\check{\mathbf{c}} \ B^2\check{\mathbf{c}} \ \dots \ B^{d-1}\check{\mathbf{c}}] \quad (8)$$

is full rank.<sup>3</sup> We concentrate on the specific scenario where the matrix  $B$  (and hence,  $A$ ) is diagonalizable, i.e.,  $B = Q\Lambda Q^{-1}$ , where  $Q \in \mathbb{R}^{d \times d}$  is an invertible matrix (hence, full rank) and  $\Lambda$  is a diagonal matrix with diagonal elements  $\{\lambda_i, 1 \leq i \leq d\}$ . For such matrices, the transpose of the observability matrix can be written as

$$\begin{aligned} (O(\check{\mathbf{c}}^T, B^T))^T &= [\check{\mathbf{c}} \ B\check{\mathbf{c}} \ B^2\check{\mathbf{c}} \ \dots \ B^{d-1}\check{\mathbf{c}}] \\ &= [QQ^{-1}\check{\mathbf{c}} \ Q\Lambda Q^{-1}\check{\mathbf{c}} \ \dots \ Q\Lambda^{d-1}Q^{-1}\check{\mathbf{c}}] \\ &= Q[\mathbf{e} \ \Lambda\mathbf{e} \ \Lambda^2\mathbf{e} \ \dots \ \Lambda^{d-1}\mathbf{e}], \end{aligned}$$

where  $\mathbf{e} = Q^{-1}\check{\mathbf{c}}$ . This can be expanded as

$$Q \begin{bmatrix} e_1 & \lambda_1 e_1 & \lambda_1^2 e_1 & \dots & \lambda_1^{d-1} e_1 \\ e_2 & \lambda_2 e_2 & \lambda_2^2 e_2 & \dots & \lambda_2^{d-1} e_2 \\ \vdots & \vdots & \vdots & \dots & \vdots \\ e_d & \lambda_d e_d & \lambda_d^2 e_d & \dots & \lambda_d^{d-1} e_d \end{bmatrix}$$

and further into

$$Q \begin{bmatrix} e_1 & & & 0 \\ & e_2 & & \\ & & \ddots & \\ 0 & & & e_d \end{bmatrix} \begin{bmatrix} 1 & \lambda_1 & \lambda_1^2 & \dots & \lambda_1^{d-1} \\ 1 & \lambda_2 & \lambda_2^2 & \dots & \lambda_2^{d-1} \\ \vdots & \vdots & \vdots & \dots & \vdots \\ 1 & \lambda_d & \lambda_d^2 & \dots & \lambda_d^{d-1} \end{bmatrix}.$$

We can establish a sufficient condition for when the observability matrix is full rank.

**THEOREM 4.4.** *Let  $\widetilde{M} = 1$  and let the elements of  $\check{\Phi} = \phi^T$  be i.i.d. from a sub-Gaussian distribution. Then, with high probability, the observability matrix is full rank when the state transition matrix is diagonalizable and its eigenvectors and eigenvalues are unique.*

*Proof.* From the discussion above, the observability matrix can be written as a product of three square matrices:  $Q$ , the matrix of eigenvectors of  $A^T$ ; a diagonal matrix with entries defined by the vector  $\mathbf{e} = Q^{-1}C^T\phi$ ; and a Vandermonde matrix defined by the vector of eigenvalues of  $A$   $\{\lambda_i, 1 \leq i \leq d\}$ . When the eigenvectors and eigenvalues are distinct, the first and last matrices are full rank. Given that the elements of  $\phi$  are i.i.d., the probability that  $e_i = 0$  is negligible and, hence, the diagonal matrix is full rank with high probability. Since the product of full rank square matrices is full rank as well, this implies that the observability matrix is full rank with high probability.  $\square$

Theorem 4.4 is intriguing, since it guarantees recovery of the state sequence even when we obtain only *one* common measurement per time instant. This is immensely useful in reducing the number of measurements required to sense a video sequence.

Interestingly, we can reduce  $\widetilde{M}$  even further. This is achieved by not obtaining common measurements at some time instants.

<sup>3</sup>There is an interesting connection to Krylov-subspace methods here. In Krylov-subspace methods, a low-rank approximation to a matrix  $K$  is obtained by forming the matrix  $[\mathbf{c} \ K\mathbf{c} \ K^2\mathbf{c} \ \dots]$  with  $\mathbf{c}$  randomly chosen. Convergence proofs for this method are closely related to Theorem 4.4. To the best of our knowledge, diagonalizability of  $K$  plays an important role in most of these proofs. The interested reader is referred to [31] for more details.



**4.3. Missing measurements: Case  $\widetilde{M} < 1$ .** If we do not obtain common measurements at some time instants, then is it still possible to obtain an estimate of the state sequence? One way to view this problem is that we have incomplete knowledge of the Hankel matrix defined in (3) and we seek to *complete* this matrix. Matrix completion, especially for low rank matrices, has received significant attention recently [6, 8, 29].

Given that the Hankel matrix  $\text{Hank}(\widetilde{\mathbf{z}}_{1:T}, q)$  in (3) is low rank for videos modeled as LDSs, we formulate the missing measurement recovery problem as one of matrix completion. Suppose that we have the common measurements only at time instants given by the index set  $\mathcal{I} \subset \{1, \dots, T\}$ , i.e., we have knowledge of  $\{\widetilde{\mathbf{z}}_i, i \in \mathcal{I}\}$ . We can recover the missing measurements by exploiting the low-rank property of  $\text{Hank}(\widetilde{\mathbf{z}}_{1:T}, q)$ . Specifically, we solve the following problem to obtain the missing measurements:

$$\min \text{rank}(\text{Hank}(\mathbf{g}_{1:T}, q)) \quad \text{s.t.} \quad \mathbf{g}_i = \widetilde{\mathbf{z}}_i, i \in \mathcal{I}.$$

However,  $\text{rank}(\cdot)$  is a non-convex function which renders the above problem NP-complete. In practice, we can solve a convex relaxation of this problem<sup>4</sup>

$$\min \|\text{Hank}(\mathbf{g}_{1:T}, q)\|_* \quad \text{s.t.} \quad \mathbf{g}_i = \widetilde{\mathbf{z}}_i, i \in \mathcal{I}, \quad (9)$$

where  $\|H\|_*$  is the nuclear norm of the matrix  $H$ , which equals the sum of its singular values. Once we fill in the missing measurements, we use (7) to recover an estimate of the state sequence.

An important quantity to characterize is the proportion of time instants where we can choose to not obtain common measurements. This amounts to developing a sampling theorem for the completion of low-rank Hankel matrices; to the best of our knowledge, there has been little theoretical work on this problem. Instead, we address it empirically in Section 6.

**5. Estimating the observation matrix.** In this section, we discuss estimation of the observation matrix  $C$  given the estimates of the state space sequence  $\widehat{\mathbf{x}}_{1:T}$ .

**5.1. Need for innovation measurements.** Given estimates of the state sequence  $\widehat{\mathbf{x}}_{1:T}$ , the matrix  $C$  is linear in the compressive measurements which enables a host of conventional  $\ell_2$ -based methods as well as  $\ell_1$ -based recovery algorithms to estimate  $C$ . However, recall that the  $C$  is a  $N \times d$  matrix and, hence, the common measurements by themselves are not enough to recover  $C$ , unless  $\widetilde{M}$  is large.

The common measurements  $\widetilde{\mathbf{z}}_{1:T}$  used in the estimation of the state sequence are measured using a time-invariant measurement matrix  $\widetilde{\Phi}$ . A time-invariant measurement matrix, by itself, is not sufficient for estimating  $C$  unless  $\widetilde{M}$  is very large. To alleviate this problem, we take additional compressive measurements of each frame using a time-varying measurement matrix. Let  $\widetilde{\mathbf{z}}_t = \widetilde{\Phi}_t \mathbf{y}_t + \omega_t = \widetilde{\Phi}_t C \mathbf{x}_t + \omega_t$ , where  $\widetilde{\mathbf{z}}_t \in \mathbb{R}^{\widetilde{M}}$  and  $\widetilde{\Phi}_t \in \mathbb{R}^{\widetilde{M} \times N}$  are the compressive measurements and the corresponding measurement matrix at time  $t$ . As mentioned earlier in Section 3, we refer to these as innovation measurements. Noting that  $C$  is a time-invariant parameter, we can collect innovation measurements over a period of time before reconstructing  $C$ . This enables a significant reduction in the number of measurements taken at each time instant.

<sup>4</sup>Historically, the use of nuclear norm-based optimization for system identification goes back to Fazel et al. [18, 19]. Since then, there has been much work towards establishing the equivalence of these two problems [6, 29].

**5.2. Structured sparsity for  $C$ .** We employ sparse priors in the recovery of the observation matrix  $C$ . For a large class of videos, the columns of  $C$  represent the dominant motion in the scene; when motion in the scene is spatially correlated, the columns of  $C$  are compressible in wavelet/DCT basis. Hence, we can potentially obtain an estimate of  $C$  by solving the following convex program:

$$(P_{\ell_1}) \quad \min \sum_{i=1}^d \|\Psi^T \mathbf{c}_i\|_1 \quad \text{s.t.} \quad \forall t, \|\mathbf{y}_t - \tilde{\Phi}_t C \hat{\mathbf{x}}_t\|_2 \leq \epsilon. \quad (10)$$

Here, we denote the columns of the matrix  $C$  as  $\mathbf{c}_i, i = 1, \dots, d$ .  $\Psi$  is a sparsifying basis for the columns of  $C$ ; we have the freedom to choose different sparsifying bases for different columns of  $C$ . In addition to this, we can use dictionary learning algorithms [23] to learn an appropriate basis where in the columns of  $C$  are sparse/compressible. When the columns of  $C$  are not sparse, the  $\ell_1$ -prior fails. For such systems, we can revert to  $\ell_2$ -based methods to recover  $C$ ; in such cases, we would typically need more measurements to recover  $C$ .

However, the convex program  $(P_{\ell_1})$  is not sufficient as-is to recover  $C$ . The reason for this stems from ambiguities in the definition of the LDS (see Section 2.3). The use of SVD for recovering the state sequence introduces an ambiguity in the estimates of the state sequence in the form of  $[\hat{\mathbf{x}}_{1:T}] \approx L^{-1}[\mathbf{x}_{1:T}]$ , where  $L$  is an invertible  $d \times d$  matrix. As a consequence, this will lead to an estimate  $\hat{C} = CL$  satisfying  $\mathbf{z} = \Phi \hat{C} \hat{\mathbf{x}}_t = \Phi(CL)(L^{-1}\mathbf{x}_t) = \Phi C \mathbf{x}_t$ . Suppose the columns of  $C$  are  $K$ -sparse (equivalently, compressible for a certain value of  $K$ ) each in  $\Psi$  with support  $\mathcal{S}_k$  for the  $k$ -th column. Then, the columns of  $CL$  are potentially  $dK$ -sparse with identical supports  $\mathcal{S} = \bigcup_k \mathcal{S}_k$ . The support is exactly  $dK$ -sparse when the  $\mathcal{S}_k$  are disjoint and  $L$  is dense. At first glance, this seems to be a significant drawback, since the overall sparsity of  $\hat{C}$  has increased to  $d^2K$  (the sparsity of  $C$  is  $dK$ ). However, this apparent increase in sparsity is alleviated by the columns having identical supports, which can be exploited in the recovery process.

Given the estimates  $\hat{\mathbf{x}}_{1:T}$ , we estimate the matrix  $C$  by solving the following convex program:

$$(P_{\ell_2-\ell_1}) \quad \min \sum_{i=1}^N \|\mathbf{s}_i\|_2 \quad \text{s.t.} \quad C = \Psi S, \quad \forall t, \|\tilde{\mathbf{z}}_t - \tilde{\Phi}_t C \hat{\mathbf{x}}_t\|_2 \leq \epsilon, \quad (11)$$

where  $\mathbf{s}_i$  is the  $i$ -th row of the matrix  $S = \Psi^T C$  and  $\Psi$  is a sparsifying basis for the columns of  $C$ . The above problem is an instance of an  $\ell_2-\ell_1$  mixed-norm optimization that promotes group sparsity; in this instance, we use it to promote group column sparsity in the matrix  $S$ , i.e., all columns have the same sparsity pattern.

There are multiple efficient ways to solve  $(P_{\ell_2-\ell_1})$ , including solvers such as *SPG-L1* [36] and model-based CoSAMP [3]. Algorithm 1 summarizes a model-based CoSAMP algorithm used for recovering the observation matrix  $C$ . The specific model used here is a union-of-subspaces model that groups each row of  $S = \Psi^T C$  into a single subspace/model. This greedy solution offers a computationally efficient alternative to the convex program  $(P_{\ell_2-\ell_1})$  at a small price in the accuracy of the result. In addition to this, in many applications, the parameters associated with the CoSAMP algorithm are far more intuitive. Specifically, the only parameter required in Algorithm 1 is the sparsity  $K$  or the expected number of non-zeros in each column of  $S = \Psi^T C$ .

**5.3. Value of  $\tilde{M}$ .** For stable recovery of the observation matrix  $C$ , we need in total  $O(dK \log(N/K))$  measurements; for a large class of practical solvers, a rule

---

**Algorithm 1:**  $\hat{C}$  = Model-based CoSAMP ( $\Psi, K, \mathbf{z}_t, \hat{\mathbf{x}}_t, \Phi_t, t = 1, \dots, T$ )

---

Notation:

$\text{supp}(\text{vec}; K)$  returns the support of  $K$  largest elements of  $\text{vec}$

$A_{|\Omega, \cdot}$  represents the submatrix of  $A$  with rows indexed by  $\Omega$  and all columns.

$A_{\cdot, |\Omega}$  represents the submatrix of  $A$  with columns indexed by  $\Omega$  and all rows.

Initialization

$\forall t, \Theta_t \leftarrow \Phi_t \Psi$

$\forall t, \mathbf{v}_t \leftarrow \mathbf{0} \in \mathbb{R}^M$

$\Omega_{\text{old}} \leftarrow \emptyset$

**while** (*stopping conditions are not met*) **do**

  Compute signal proxy:

$R = \sum_t \Theta_t^T \mathbf{v}_t \hat{\mathbf{x}}_t^T$

  Compute energy in each row:

$k \in [1, \dots, N], \mathbf{r}(k) = \sum_{i=1}^d R^2(k, i)$

  Support identification and merger:

$\Omega \leftarrow \Omega_{\text{old}} \cup \text{supp}(\mathbf{r}; 2K)$

  Least squares estimation:

    Find  $A \in \mathbb{R}^{|\Omega| \times d}$  that minimizes  $\sum_t \|\mathbf{z}_t - (\Theta_t)_{|\cdot, \Omega} A \hat{\mathbf{x}}_t\|_2$

$B_{|\Omega, \cdot} \leftarrow A, B_{|\Omega^c, \cdot} \leftarrow 0$

  Pruning support:

$k \in [1, \dots, N], \mathbf{b}(k) = \sum_{i=1}^d B^2(k, i)$

$\Omega \leftarrow \text{supp}(\mathbf{b}; K), S_{|\Omega, \cdot} \leftarrow B_{|\Omega, \cdot}, S_{|\Omega^c, \cdot} \leftarrow 0$

  Form new estimate of  $C$ :

$\hat{C} \leftarrow \Psi S$

  Update residue:

$\forall t, \mathbf{v}_t \leftarrow \mathbf{z}_t - \Theta_t S \hat{\mathbf{x}}_t$

$\Omega_{\text{old}} \leftarrow \Omega$

**end**

---

of thumb is  $4dK \log(N/K)$ . Given that we measure  $\widetilde{M}$  time-varying compressive measurements at each time instant, over a period of  $T$  time instants, we have  $\widetilde{M}T$  compressive measurements for estimating  $C$ . Hence, for stable recovery of  $C$ , we need approximately

$$\widetilde{M}T = 4dK \log(N/K) \implies \widetilde{M} = 4 \frac{dK}{T} \log(N/K). \quad (12)$$

This indicates extremely favorable operating scenarios for the CS-LDS framework, especially when  $T$  is large (as in high frame rate capture). Let  $T = \tau f_s$ , where  $\tau$  is the time duration of the video in seconds and  $f_s$  is the sampling rate of the measurement device. The number of compressive measurements required in this case is  $\widetilde{M} = 4 \frac{dK}{\tau f_s}$ . Given that the complexity of the LDS typically (however, not always) depends on  $\tau$ , for a fixed  $\tau$  the number of measurements required to estimate  $C$  decreases as  $1/f_s$  as the sampling rate  $f_s$  is increased. Indeed, as the sampling rate  $f_s$  increases,  $\widetilde{M}$  can be decreased while keeping  $Mf_s$  constant. This will ensure that (12) is satisfied, enabling stable recovery of  $C$ .

**5.4. Mean + LDS.** In many instances, a dynamical scene is modeled better as an LDS over a static background, that is,  $\mathbf{y}_t = C\mathbf{x}_t + \mu$ . This can be handled with two small modifications to the algorithm described in Section 5.2. First, the state sequence  $[\hat{\mathbf{x}}_{1:T}]$  is obtained by performing an SVD on the matrix  $\text{Hank}(\tilde{\mathbf{z}}_{1:T}, d_{\text{guess}})$  modified such that each row sums to zero. This works under the assumption that the sample mean of  $\tilde{\mathbf{z}}_{1:T}$  is equal to  $\tilde{\Phi}\mu$ , the compressive measurement of  $\mu$ . Second, given that the support of  $\mu$  need not be similar to that of  $C$ , the ensuing convex program can be reformulated as

$$(P_{\mu, \ell_2 - \ell_1}) \min \|\Psi^T \mu\|_1 + \sum_{i=1}^N \|\mathbf{s}_i\|_2 \quad \text{s.t. } C = \Psi S, \forall t, \|\tilde{\mathbf{z}}_t - \tilde{\Phi}_t(\mu + C\hat{\mathbf{x}}_t)\|_2 \leq \epsilon. \quad (13)$$

As with the convex formulation, the model-based CoSAMP algorithm described in Algorithm 1 can be modified to incorporate the mean term  $\mu$ ; an additional modification here is the requirement to specify a priori the sparsity of the mean  $K_\mu = \|\Psi^T \mu\|_0$ .

**6. Experiments.** We present a range of experiments validating various aspects of the CS-LDS framework. We use permuted noiselets [13] for the measurement matrices, since they have a fast scalable implementation. We use the term *compression ratio*  $N/M$  to denote the reduction in the number of measurements as compared to the Nyquist rate. Finally, we use the reconstruction SNR to evaluate the recovered videos. Given the ground truth video  $\mathbf{y}_{1:T}$  and a reconstruction  $\hat{\mathbf{y}}_{1:T}$ , the reconstruction SNR in dB is defined by

$$10 \log_{10} \left( \frac{\sum_{t=1}^T \|\mathbf{y}_t\|_2^2}{\sum_{t=1}^T \|\mathbf{y}_t - \hat{\mathbf{y}}_t\|_2^2} \right).$$

We compare CS-LDS against *frame-by-frame* CS, where each frame of the video is recovered separately using conventional CS techniques. We use the term *Oracle LDS* when the parameters and video reconstruction are obtained by operating on the original data itself. Oracle LDS estimates the parameters using a rank- $d$  approximation of the ground truth data. The reconstruction SNR of the oracle LDS gives an upper bound on the achievable SNR. Finally, the ambiguity in the observation matrix (due to non-uniqueness of the SVD based factorization) as estimated by Oracle LDS and CS-LDS is resolved by finding the best  $d \times d$  linear transformation that registers the two estimates.

**6.1. State sequence estimation.** We first provide empirical verification of the results derived in Sections 4.1 and 4.2. It is worth noting that, in the absence of noise, Theorem 4.4 suggests exact recovery of the state sequence. In practice, it is important to check the robustness of the estimate to measurement noise. Figure 2(a) analyzes the performance of the state space estimation for different values of the number of common measurements  $\tilde{M}$  and different SNRs of the measurement noise. We define input SNR in dB as  $10 \log_{10} ((\sum \|\mathbf{y}_t\|_2^2)/(T\sigma^2))$ , where  $\sigma$  is the standard deviation of the noise. Here, we consider the scenario when  $\tilde{M} \geq 1$ . The underlying state space dimension is  $d = 10$  with  $T = 500$  frames. As expected, for low SNRs, the reconstruction SNR is very high even for small values of  $\tilde{M}$ . In addition to this, the accuracy at  $\tilde{M} = 1$  is acceptable, especially at low SNRs.

Next, we validate the implications of Section 4.3, where we discuss the scenario of  $\tilde{M} < 1$  by simulating various proportions of missing common measurements. Figure 2(b) shows reconstruction SNR for the Hankel matrix in (3) for varying amounts of

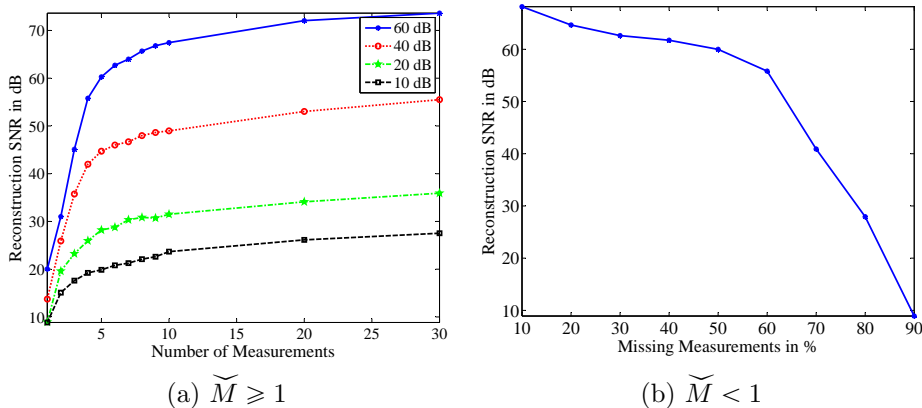


FIG. 2. Accuracy of state sequence estimation from common measurements. Shown are aggregate results over 100 Monte-Carlo runs for an LDS with  $d = 10$  and  $T = 500$ . For each Monte-Carlo run, the system matrices and the state sequence were generated randomly. (a) Reconstruction SNR as a function of the number of common measurements  $\tilde{M}$  per frame. Each curve is for a different level of measurement noise as measured using input SNR. For low noise levels, we obtain a good reconstruction SNR ( $> 20$  dB) even at  $\tilde{M} = 1$ ; this hints at very high compression ratios. (b) Reconstruction SNR of the Hankel matrix for the scenario with missing common measurements. We can estimate the Hankel matrix very accurately even at 80% missing measurements. This suggests immense flexibility in the implementation of the CS-LDS system.

missing measurements. We recover the Hankel matrix by solving (9) using CVX [20]. Figure 2(b) demonstrates a very high reconstruction SNR even at a very high rate of missing measurements. As mentioned earlier, not having to sense common measurements at all frames is very useful, since we can stagger our acquisition of common and innovation measurements. In theory, this enables a measurement strategy where we need to sense only one measurement per frame of the video without having to group consecutive measurements of the SPC. Hence, we can aim to reconstruct videos at the sampling rate of the SPC. To the best of our knowledge, this is the first video CS acquisition design capable of doing this.

**6.2. Dynamic Textures.** Our test dataset comprises of videos from the DynTex dataset [28]. We used the mean+LDS model from Section 5.4 for all the video CS experiments with the 2D DCT as the sparsifying basis for the columns of  $C$  and 2D wavelets as the sparsifying basis for the mean. We used the model-based CoSAMP solver in Algorithm 1 for these results, since it provides explicit control of the sparsity of the mean and the columns of  $C$ . We used (12) as a guide to select these values.

Figure 3 shows video reconstruction of a dynamic texture from the DynTex dataset [28]. Reconstruction results are under a compression  $N/M = 234$ ; this is an operating point where a frame-to-frame CS recovery is completely infeasible. However, the dynamic component of the scene is relatively small ( $d = 20$ ), which allows us to recover the video from relatively few measurements. The reconstruction SNR of the recovered videos shown are as follows: Oracle LDS = 24.97 dB, frame-to-frame CS = 11.75 dB and CS-LDS = 22.08 dB.

Figure 4 shows the reconstruction of a video, of 6 blinking LED lights, from the DynTex dataset. We show reconstruction results at different compression ratios as well as different image resolutions. It is noteworthy that, even at a 100x compression, the reconstruction at a resolution of  $256 \times 256$  pixels preserves fine details.

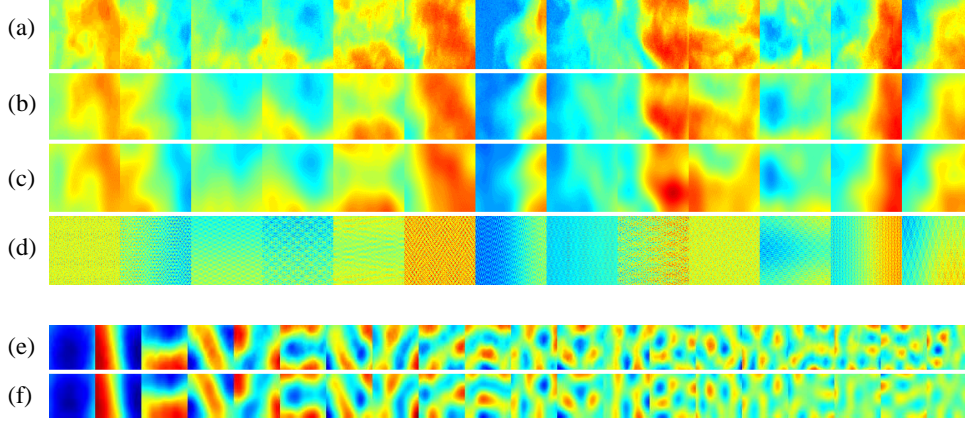


FIG. 3. Reconstruction of a fire texture of length 250 frames and resolution of  $N = 128 \times 128$  pixels. (a-d) Sampling of frames of the (a) Ground truth video, (b) Oracle LDS reconstruction, (c) CS-LDS reconstruction, and (d) naive frame-to-frame CS reconstruction. The CS-LDS reconstruction closely resembles the Oracle LDS result. For the CS-LDS results, compressive measurements were obtained at  $\tilde{M} = 30$  and  $\tilde{M} = 40$  measurements per frame, there by giving a compression ratio of  $234 \times$ . Reconstruction was performed with  $d = 20$  and  $K = 30$ . (e) Ground truth observation matrix  $C$ . (f) CS-LDS estimate of the observation matrix  $\hat{C}$ . In (e) and (f), the column of the observation matrix is visualized as an image. Both the frames of the videos and the observation matrices are shown in false-color for better contrast.

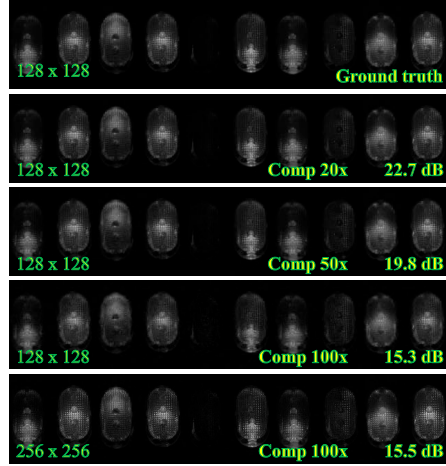


FIG. 4. Reconstruction of a video comprising of 6 blinking LED lights. We used  $d = 7$ ,  $\tilde{M} = 3d$ , and  $\tilde{M}$  chosen based on the overall compression ratio  $N/(\tilde{M} + \tilde{M})$ . Each row shows a sampling of frames of the video reconstructed at a different compression ratios. Inset in each row is the resolution of the video used as well as the compression at sensing and the reconstruction SNR. While performance degrades with increasing compression, it also gains significantly for higher dimensional data; the reconstruction at  $256 \times 256$  pixels preserves finer details.

**Performance with measurement noise:** We validate the performance of our recovery algorithm under various amounts of measurement noise. Note that the columns of  $C$  with larger singular values are, inherently, better conditioned to deal with this measurement error. The columns corresponding to the smaller singular values are invariably estimated with higher error. Figure 5 shows the performance of the recov-

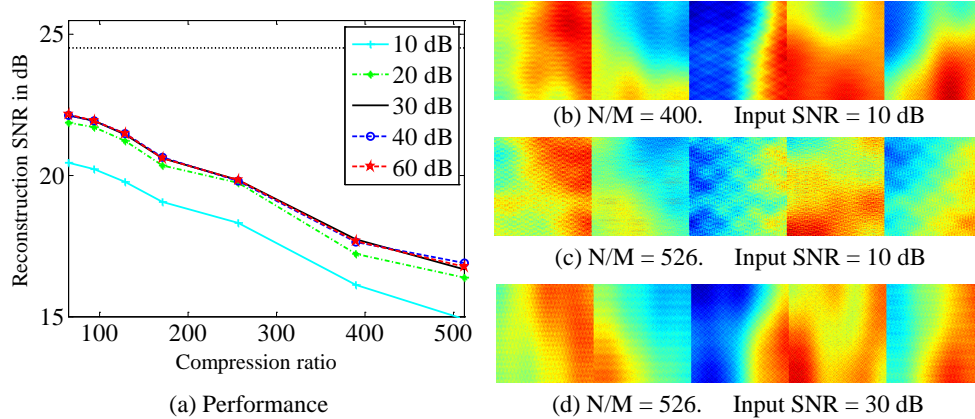


FIG. 5. Resilience of the CS-LDS framework to measurement noise. (a) Performance plot charting the reconstruction SNR as a function of compression ratio  $N/M$ . Each curve is for a different level of measurement noise as measured using and input SNR. Reconstruction SNRs were computed using 32 Monte-Carlo simulations. The “black-dotted” line shows the reconstruction SNR for an  $d = 20$  Oracle LDS. (b-d) Snapshots of video frames at various operating points. The dynamic texture of Fig. 3 was used for this result.

ery algorithm for various levels of measurement noise. The effect of the measurement noise on the reconstructions is perceived only at low input SNRs. In part, this robustness to measurement noise is due to the LDS model mismatch dominating the reconstruction error at high input SNRs. As the input SNR drops significantly below the model mismatch term, predictably, it starts influencing the reconstructions more. This provides a certain amount of flexibility in the design of potential CS-LDS cameras.

**Gallery of results:** Finally, in Figure 6, we demonstrate performance of the CS-LDS methodology for sensing and reconstructing a wide range of videos. The reader is directed to the supplemental material as well as the project webpage [2] for animated videos of these results.

**6.3. Hyperspectral imaging using CS-LDS.** The CS-LDS framework can be applied to any data that is subspace compressible; in this regard, it can be used to sense data other than video. One such example of this is sensing hyperspectral data using CS-LDS; in contrast to video, where we consider image variations with time, hyperspectral data involves imaging across spectral bands. Hyperspectral data has been shown to lie on subspaces [10]; this occurs due to the alignment of texture edges across spectral bands. One hardware implementation of CS-LDS for hyperspectral data involves a color-wheel in front of an SPC with a broadband sensor. If the optical filters on the color-wheel have a narrow passband, then we can isolate spectral bands and treat them much like the frames of a video. An alternate implementation can be obtained by using a spectrometer along with a micro-mirror device.

Hyperspectral data do not necessarily exhibit smoothness across spectral bands. Hence, we model the spectral bands as linear systems without any dynamics across the spectral bands (and without the additional term for the mean vector). We used the convex formulation in (11) for the hyperspectral reconstructions. Figure 7 showcases reconstruction results for a hyperspectral data cube along with comparisons with naive CS (where each spectral band is reconstructed separately) as well as group-



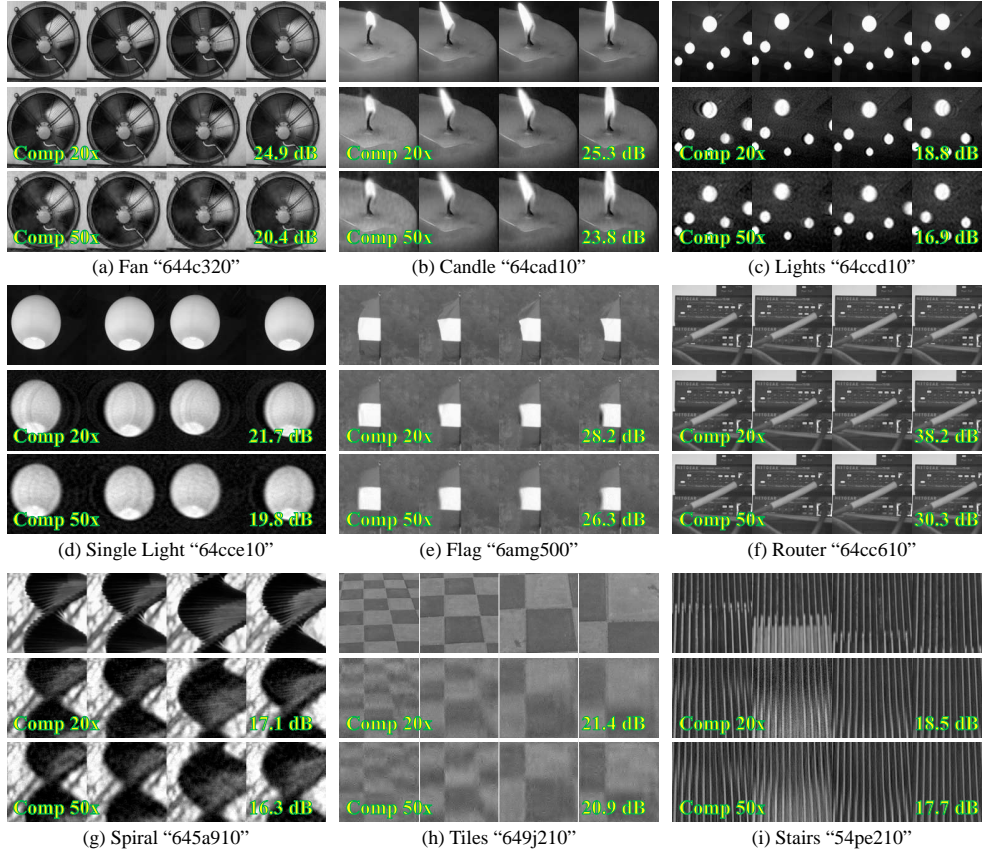


FIG. 6. A gallery of reconstruction results using the CS-LDS framework. Each sub-figure (a-i) shows reconstruction results for a different video. The three rows of each sub-figure correspond to, from top-bottom, the ground truth video and CS-LDS reconstructions at compression ratios of 20 $\times$  and 50 $\times$ . Each column is a frame of the video and its reconstruction. Inset on each reconstruction is the reconstruction SNR for that result. All videos are from the DynTex dataset [28] downsampled at a spatial resolution of 128  $\times$  128 pixels. The “code” in quotes refer to the name of the sequence in the database. For all videos,  $d = 15$  and  $\tilde{M} = 3d$ . The interested reader is directed to the project webpage [2] and the supplemental material for videos of these results.

sparse CS — where a group sparsity prior is used across spectral bands. We see that CS-LDS outperforms both of the straw-man algorithms. As discussed in Section 5.3, CS-LDS achieves higher compression ratios when applied on longer sequences. For hyperspectral data, this corresponds to having a large number of spectral bands. Figure 8 showcases reconstruction result on a hyperspectral cube from the AIRIBRAD dataset [1]. The data consists of 2301 spectral bands, each with a spatial resolution of 128  $\times$  64 pixels. The reconstructions obtained using CS-LDS are stable over a large range of compression ratios as well as parameter values.

**6.4. Application in activity analysis.** As mentioned in Section 2.3, LDSs are often used in classification problems, especially in the context of scene/activity analysis. A key experiment in this context is to check if the CS-LDS framework recovers videos that are sufficiently informative for such applications. To this end, we experiment with two different activity analysis datasets: the UCSD Traffic Dataset



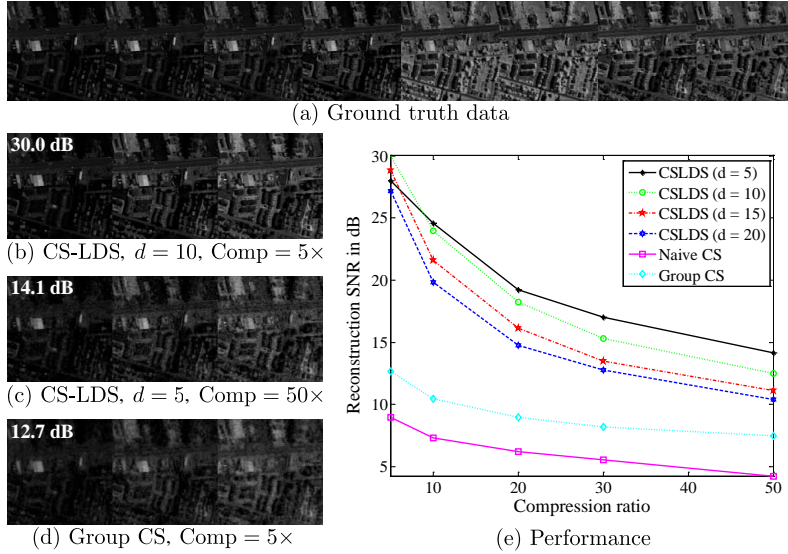


FIG. 7. *Reconstruction of a hyperspectral datacube with 128 spectral bands; the image at each spectral band has  $128 \times 128$  pixels. (a) Sampling of the spectral bands of the data. (b – d) Reconstruction results of CS-LDS at two different operating points and a conventional CS algorithm with group-sparse prior. Inset in each sub-figure is the reconstruction SNR in dB. (e) We compare performance of various algorithms for varying compression ratios. We used 2D wavelets as the sparsifying basis.*

[11] and the UMD Human Activity Dataset [40].

**The UCSD Traffic Dataset** [11] consists of 254 videos capturing traffic of three types: light, moderate, and heavy. Each video is of length 50 frames at a resolution of  $64 \times 64$  pixels. Figure 9 shows the reconstruction results on a traffic sequence from the dataset. We perform a classification experiment of the videos into these three categories. There are four different train-test scenarios provided with the dataset. For comparison, we also perform the same experiments with fitting the LDS model on the original frames (Oracle LDS). We perform classification at two different values of the state space dimension  $d$  and at a fixed compression ratio of  $25\times$ .

**The UMD Human Activity Dataset** [40] consists 100 videos, each of length 80 frames, depicting 10 different activities: *pickup object*, *jog*, *push*, *squat*, *wave*, *kick*, *bend*, *throw*, *turn around* and *talk on cellphone*. Each activity was repeated 10 times, so there were a total of 100 sequences in the dataset. As with the traffic experiment, we use an LDS model on the image intensity values without any feature extraction. Images were cropped to contain the human and resized to  $330 \times 300$ . The state space dimension was fixed at  $d = 5$  and the compression was varied from  $50\times$  to  $200\times$ .

For both datasets, we used the Procrustes distance [12] between the column spaces of the observability matrices in the design of a nearest-neighbor classifier. Given the observability matrix  $O(C, A)$  defined in (6), let  $Q$  be an orthonormal matrix such that  $\text{span}(Q) = \text{span}(O(C, A))$ . Given two LDSs, the squared Procrustes distance between them is given by

$$d^2(Q_1, Q_2) = \min_{R \in \mathbb{R}^{d \times d}} \text{tr}(Q_1 - Q_2 R)^T (Q_1 - Q_2 R),$$

where  $\text{span}(Q_1) = \text{span}(O(C_1, A_1))$  and  $\text{span}(Q_2) = \text{span}(O(C_2, A_2))$ . We use this

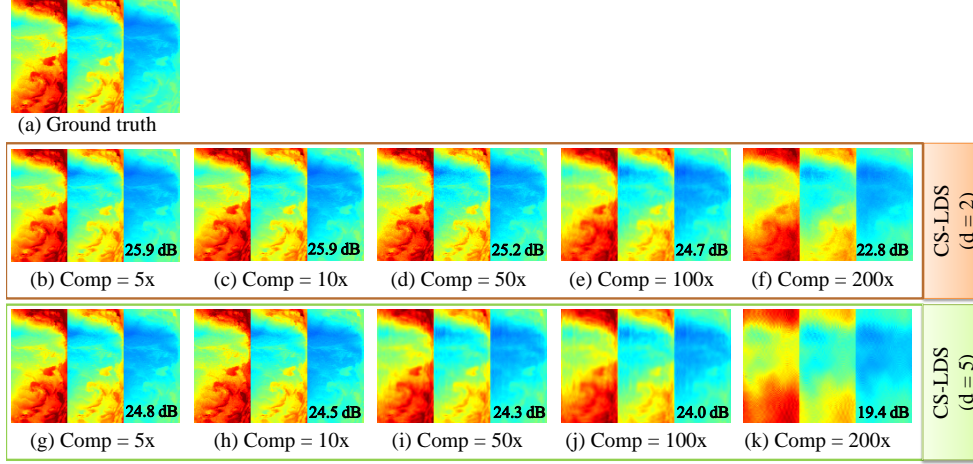


FIG. 8. Reconstruction of a hyperspectral datacube with 2301 spectral bands; the image at each spectral band has  $128 \times 64$  pixels. (a) Sampling of the three spectral bands of the data. (b – f) Reconstruction results of CS-LDS with  $d = 2$  and at various compression ratios. (g – k) Reconstruction results of CS-LDS with  $d = 5$  and at various compression ratios. Inset in each sub-figure is the reconstruction SNR in dB. We used 2D wavelets as the sparsifying basis. We use a false-colormap for enhanced contrast and better visualization of subtle details.

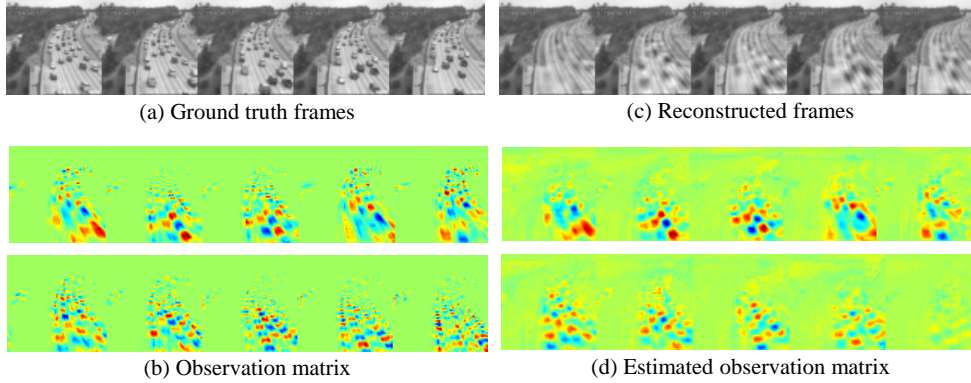


FIG. 9. Reconstructions of a traffic scene of  $N = 64 \times 64$  pixels at a compression ratio  $N/M = 25$ , with  $d = 15$  and  $K = 40$ . (a, c) Sampling of the frames of the ground truth and reconstructed video. (b, d) The first ten columns of the observation matrix  $C$  and the estimated matrix  $\hat{C}$ ; both are shown in false color for improved contrast. The quality of reconstruction and LDS parameters is sufficient for capturing the flow of traffic as seen in the classification results in Table 1.

distance function in a nearest neighbor classifier in the classification experiment. We performed a leave-one-execution-out test. The results are summarized in Tables 1 and 2. In both classification experiments, the CS-LDS framework obtained a classification performance that is comparable to the Oracle LDS. For the UMD Human Activity Dataset, both Oracle LDS and CS-LDS obtained a perfect classification score of 100% up to a compression ratio of  $50\times$ . This suggests that the CS-LDS framework should be extremely useful in a wide range of applications beyond just video recovery.

**7. Discussion.** In this paper, we have proposed a framework for the compressive acquisition of dynamic scenes modeled as LDSs. In particular, this paper emphasizes

TABLE 1  
*Classification results (in %) on the UCSD Traffic Dataset*

	Expt 1	Expt 2	Expt 3	Expt 4
<b>(d = 10)</b>				
Oracle LDS	85.71	85.93	87.5	92.06
CS-LDS	84.12	87.5	89.06	85.71
<b>(d = 5)</b>				
Oracle LDS	77.77	82.81	92.18	80.95
CS-LDS	85.71	73.43	78.1	76.1

TABLE 2  
*Classification results (in %) on the UMD Human Activity Database*

Activity	100×	150×	200×
Pickup Object	100	100	100
Jog	100	100	90
Push	100	90	50
Squat	90	100	100
Wave	100	100	60
Kick	100	90	80
Bend	100	100	100
Throw	100	100	90
Turn Around	100	100	100
Talk on Cellphone	100	20	10
Average	94	90	78

the power of predictive/generative video models. In this regard, we have shown that a strong model for the scene dynamics enables stable video reconstructions at very low measurement rates. In particular, it enables the estimation of the state sequence associated with a video even at fractional number of common measurements per video frame ( $\bar{M} \leq 1$ ). The use of CS-LDS for dynamic scene modeling and classification also highlights the purposive nature of the framework.

**Connection to affine-rank minimization:** The pioneering work of Fazel [17] in developing convex optimization techniques to system identification problems has interesting parallels to the ideas proposed in this paper. One of the key ideas espoused in [17] is that, when the video sequence  $\mathbf{y}_{1:T}$  is an LDS, the block Hankel matrix  $\text{Hank}(\mathbf{y}_{1:T}, q)$  is low rank. When we have linear measurements of the video frames, we can solve an affine-rank problem to recover the video. However, such methods optimize on the Hankel matrix directly and lead to computationally infeasible designs even for videos of very small dimensions. In contrast, CS-LDS has been shown to be fast and computationally feasible for very large videos involving millions of variables. The key is our two-step solution that isolates the space of unknowns into two manageable sets and solves for each separately.

**Universality:** An attractive property of random matrix-based CS measurement is the universality of the measurement process. Universality implies that the sensing process is independent of the subsequent reconstruction algorithm. This makes the sensing design “future-proof”; for such systems, if we devise a more sophisticated and powerful recovery algorithm in the future, then we do not need to redesign the cam-

era or the sensing framework. The CS-LDS framework violates this property. The two-step measurement process of Section 3, which is key to breaking the bilinearity introduced by the LDS prior, implies that the CS-LDS design is not universal. An intriguing direction for future research is the design of a universal CS-LDS measurement process.

**Online tracking:** We have made the assumption of a static observation matrix  $C$ . However, as the length of the video increases, the assumption of a static  $C$  is satisfied only by increasing the state space dimension. An alternate approach is to allow for a time-varying observation matrix  $C(t)$  and track it from the compressive measurements. This would give us the benefit of a low state space dimension and yet, be accurate when we sense for long durations.

**Beyond LDS:** While the CS-LDS framework makes a compelling case study of LDSs for video CS, its applicability to arbitrary videos is limited. In particular, it does not extend to simple non-stationary scenes such as people walking or panning cameras (see the result associated with Figure 6(h)). This motivates the search for models more general than LDS. In this regard, a promising line of future research is to leverage our models from the video compression literature for CS recovery.

**Acknowledgments.** ACS and RGB were partially supported by the grants NSF CCF-0431150, CCF-0728867, CCF-0926127, CCF-1117939, ARO MURI W911NF-09-1-0383, W911NF-07-1-0185, DARPA N66001-11-1-4090, N66001-11-C-4092, N66001-08-1-2065, and AFOSR FA9550-09-1-0432.

RC was partially supported by the Office of Naval Research under the Grant N000141210124.

## REFERENCES

- [1] *AIRS Infrared level 1b data set*. URL = <http://disc.sci.gsfc.nasa.gov/AIRS/data-holdings/by-data-product/airsL1B.Rad.shtml>
- [2] *CS-LDS Project webpage*. URL = <http://www.ece.rice.edu/~as48/research/cslds>.
- [3] R. G. BARANIUK, V. CEVHER, M. F. DUARTE, AND C. HEGDE, *Model-based compressive sensing*, IEEE Trans. Inf. Theory, 56 (2010), pp. 1982–2001.
- [4] R. G. BARANIUK, M. DAVENPORT, R. DEVORE, AND M. WAKIN, *A simple proof of the restricted isometry property for random matrices*, Constr. Approx., 28 (2008), pp. 253–263.
- [5] R. W. BROCKETT, *Finite Dimensional Linear Systems*, Wiley, 1970.
- [6] E. J. CANDÈS AND B. RECHT, *Exact matrix completion via convex optimization*, Found. Comp. Math., 9 (2009), pp. 717–772.
- [7] E. J. CANDÈS, J. ROMBERG, AND T. TAO, *Robust uncertainty principles: Exact signal reconstruction from highly incomplete frequency information*, IEEE Trans. Inf. Theory, 52 (2006), pp. 489–509.
- [8] E. J. CANDÈS AND T. TAO, *The power of convex relaxation: Near-optimal matrix completion*, IEEE Trans. Inf. Theory, 56 (2010), pp. 2053–2080.
- [9] V. CEVHER, A. C. SANKARANARAYANAN, M. F. DUARTE, D. REDDY, R. G. BARANIUK, AND R. CHELLAPPA, *Compressive sensing for background subtraction*, in Euro. Conf. Comp. Vision, Oct. 2008.
- [10] A. CHAKRABARTI AND T. ZICKLER, *Statistics of real-world hyperspectral images*, in IEEE Conf. Comp. Vision and Pattern Recog, June 2011.
- [11] A. B. CHAN AND N. VASCONCELOS, *Probabilistic kernels for the classification of auto-regressive visual processes*, in IEEE Conf. Comp. Vision and Pattern Recog, June 2005.
- [12] Y. CHIKUSE, *Statistics on special manifolds*, Springer Verlag, 2003.
- [13] R. COIFMAN, F. GESHWIND, AND Y. MEYER, *Noiselets*, Appl. Comp. Harm. Anal., 10 (2001), pp. 27–44.
- [14] D. L. DONOHO, *Compressed sensing*, IEEE Trans. Inf. Theory, 52 (2006), pp. 1289–1306.
- [15] G. DORETTO, A. CHIUSO, Y. N. WU, AND S. SOATTO, *Dynamic textures*, Intl. J. Comp. Vision, 51 (2003), pp. 91–109.

- [16] M. F. DUARTE, M. A. DAVENPORT, D. TAKHAR, J. N. LASKA, T. SUN, K. F. KELLY, AND R. G. BARANIUK, *Single-pixel imaging via compressive sampling*, IEEE Signal Process. Mag., 25 (2008), pp. 83–91.
- [17] M. FAZEL, *Matrix rank minimization with applications*, PhD thesis, Stanford University, 2002.
- [18] M. FAZEL, H. HINDI, AND S. P. BOYD, *A rank minimization heuristic with application to minimum order system approximation*, in IEEE Amer. Control Conf., June 2001.
- [19] ———, *Log-det heuristic for matrix rank minimization with applications to hankel and euclidean distance matrices*, in IEEE Amer. Control Conf., June 2003.
- [20] M. GRANT AND S. BOYD, *CVX: Matlab software for disciplined convex programming, version 1.21*, Available at <http://cvxr.com/cvx>, (2011).
- [21] J. HAUPT AND R. NOWAK, *Signal reconstruction from noisy random projections*, IEEE Trans. Inf. Theory, 52 (2006), pp. 4036–4048.
- [22] Y. HITOMI, J. GU, M. GUPTA, T. MITSUNAGA, AND S. K. NAYAR, *Video from a single coded exposure photograph using a learned over-complete dictionary*, in IEEE Intl. Conf. Comp. Vision, Nov. 2011.
- [23] K. KREUTZ-DELGADO, J. F. MURRAY, B. D. RAO, K. ENGAN, T. W. LEE, AND T. J. SEJNOWSKI, *Dictionary learning algorithms for sparse representation*, Neural Comp., 15 (2003), pp. 349–396.
- [24] S. K. NAYAR, V. BRANZOI, AND T. E. BOULT, *Programmable imaging: Towards a flexible camera*, Intl. J. Comp. Vision, 70 (2006), pp. 7–22.
- [25] D. NEEDELL AND J. A. TROPP, *Cosamp: Iterative signal recovery from incomplete and inaccurate samples*, Appl. Comp. Harm. Anal., 26 (2009), pp. 301–321.
- [26] J. Y. PARK AND M. B. WAKIN, *A multiscale framework for compressive sensing of video*, in Pict. Coding Symp., May 2009.
- [27] Y. C. PATI, R. REZAIEFAR, AND P. S. KRISHNAPRASAD, *Orthogonal matching pursuit: Recursive function approximation with applications to wavelet decomposition*, in Asilomar Conf. Signals Sys. Comp., Nov. 1993.
- [28] R. PÉTERI, S. FAZEKAS, AND M. J. HUISKES, *DynTex: A comprehensive database of dynamic textures*, Pattern Recog. Letters, 31 (2010), pp. 1627–1632.
- [29] B. RECHT, M. FAZEL, AND P. A. PARRILO, *Guaranteed minimum-rank solutions of linear matrix equations via nuclear norm minimization*, arXiv:0706.4138, (2007).
- [30] D. REDDY, A. VEERARAGHAVAN, AND R. CHELLAPPA, *P2C2: Programmable pixel compressive camera for high speed imaging*, in IEEE Conf. Comp. Vision and Pattern Recog, June 2011.
- [31] Y. SAAD, *Krylov subspace methods for solving large unsymmetric linear systems*, Math. Comput., 37 (1981), pp. 105–126.
- [32] P. SAISAN, G. DORETTO, Y. WU, AND S. SOATTO, *Dynamic texture recognition*, in IEEE Conf. Comp. Vision and Pattern Recog, Dec. 2001.
- [33] A. C. SANKARANARAYANAN, P. TURAGA, R. BARANIUK, AND R. CHELLAPPA, *Compressive acquisition of dynamic scenes*, in Euro. Conf. Comp. Vision, Sep. 2010.
- [34] S. SOATTO, G. DORETTO, AND Y. N. WU, *Dynamic textures*, in IEEE Intl. Conf. Comp. Vision, July 2001.
- [35] P. TURAGA, A. VEERARAGHAVAN, AND R. CHELLAPPA, *Unsupervised view and rate invariant clustering of video sequences*, Comp. Vision and Image Understd., 113 (2009), pp. 353–371.
- [36] E. VAN DEN BERG AND M. P. FRIEDLANDER, *Probing the pareto frontier for basis pursuit solutions*, SIAM J. Scientific Comp., 31 (2008), pp. 890–912.
- [37] P. VAN OVERSCHEE AND B. DE MOOR, *N4SID: Subspace algorithms for the identification of combined deterministic-stochastic systems*, Automatica, 30 (1994), pp. 75–93.
- [38] N. VASWANI, *Kalman filtered compressed sensing*, in IEEE Conf. Image Process., Oct. 2008.
- [39] N. VASWANI AND W. LU, *Modified-CS: Modifying compressive sensing for problems with partially known support*, in Intl. Symp. Inf. Theory, June 2009.
- [40] A. VEERARAGHAVAN, R. CHELLAPPA, AND A. K. ROY-CHOWDHURY, *The function space of an activity*, in IEEE Conf. Comp. Vision and Pattern Recog, June 2006.
- [41] A. VEERARAGHAVAN, D. REDDY, AND R. RASKAR, *Coded strobing photography: Compressive sensing of high speed periodic events*, IEEE Trans. Pattern Anal. Mach. Intell., 33 (2011), pp. 671–686.
- [42] M. B. WAKIN, J. N. LASKA, M. F. DUARTE, D. BARON, S. SARVOTHAM, D. TAKHAR, K. F. KELLY, AND R. G. BARANIUK, *Compressive imaging for video representation and coding*, in Pict. Coding Symp., Apr. 2006.
- [43] M. B. WAKIN, B. M. SANANAJI, AND T. L. VINCENT, *On the observability of linear systems from random, compressive measurements*, in IEEE Conf. on Decision and Control, Dec. 2010.